CrossMark

J. Fluid Mech. (2015), *vol.* 775, *pp.* 266–287. © Cambridge University Press 2015
doi:10.1017/jfm.2015.298

Separation of upslope flow over a uniform slope

C. M. Hocut[1], D. Liberzon[1] and H. J. S. Fernando[1,2,†]

[1]Environmental Fluid Dynamics Laboratories, Department of Civil and Environmental Engineering and Earth Sciences, University of Notre Dame, Notre Dame, IN 46556, USA

[2]Department of Aerospace and Mechanical Engineering, University of Notre Dame, IN 46556, USA

(Received 23 July 2014; revised 1 April 2015; accepted 21 May 2015;
first published online 23 June 2015)

Motivated by the importance of understanding mountain weather during periods of thermal convection, a laboratory study was conducted to investigate the separation of an upslope (anabatic) flow on a two-dimensional heated mountainous slope in the absence of a background mean flow. Three flow regimes were identified. In the first, at slope angles β larger than a critical value $\beta_c \approx 20°$, the separated flow generated a rising plume completely fed by the anterior upslope flow. For this case, a simple model based on a balance between the opposing vorticities of baroclinicity and shear was proposed to predict the location of the separation point relative to the mountain base. The model also predicts the velocity and length scales at separation as well as those of the rising plume after separation. In the second regime, $10° < \beta \leqslant \beta_c$, the volume flow of the separated plume was not fully supplied by the upslope flow, requiring entrainment of additional ambient fluid at the base of the plume source. The third regime occurred when $\beta \leqslant 10°$, wherein the plume almost completely engulfed the slope, similar to a buoyant plume emanating from a source of finite dimensions, thus overshadowing the upslope flow. Measurements of the separation point conducted during the MATERHORN field research program were consistent with the results of the laboratory experiments and modelling.

Key words: atmospheric flows, meteorology, topographic effects

1. Introduction

Flow separation from heated mountain slopes has been a topic of considerable interest because of its relevance to weather prediction in mountainous terrain. In particular, heat carried by the separated flow as well as small-scale features associated with flow separation are crucial for predicting deep convection, precipitation, moisture distribution and unsteady phenomena surrounding orographic features (Banta 1984; Hanley *et al.* 2011). Excessive precipitation over steep and high mountains in mesoscale as well as climate models is a well-known problem, which has been attributed to the difficulties of parameterizing flow separation over sloping boundaries, especially the sub-grid heat ventilation by separated upslope flows (Chao 2012). Without proper ventilation, the heat flux and slope flows are overestimated, which together with excessive moisture transport lead to erroneous precipitation predictions.

† Email address for correspondence: Harindra.J.Fernando.10@nd.edu

https://doi.org/10.1017/jfm.2015.298 Published online by Cambridge University Press

In the context of urban fluid mechanics, more than 70 % of the world's cities are in valleys surrounded by complex topography, and the upslope (or anabatic) flows that occur during the daytime transport urban pollution plumes toward mountainous suburbia (Ellis *et al.* 2000). The fate of pollutants is largely dependent on whether the upslope flow separates or not. When the separation occurs, pollutants are lofted to regional flow or form elevated recirculating flows within the convective boundary layer (Lu & Turco 1994; Reuten *et al.* 2005; Reuten, Steyn & Allen 2007; De Wekker 2008; Fernando *et al.* 2010; Serafin & Zardi 2010*a*,*b*), whereas in attached flows there is a propensity for pollutants to return back to the urban area with the downslope (katabatic) flow at night (Fernando *et al.* 2001). In aviation, the flow separation in the lee or windward side of the mountains is a key issue of safety (Politovich *et al.* 2011). General aspects of flow in complex terrain are extensively discussed in Barry (1992), Whiteman (2000) and Fernando (2010).

In predictive models, flow separation over slopes is sensitive to the details of the turbulent models employed (Mason 1987; Moreira *et al.* 2012), and hence an understanding of the underlying processes is vital for developing turbulence closure for numerical models. While a substantial number of theoretical, numerical and laboratory studies have been conducted on flow over mountains under stable and neutral conditions (Taylor & Teunissen 1987; Baines 1995; Raupach & Finnigan 1997; Belcher & Hunt 1998), there are few fundamental studies on flow separation under convective conditions. The heating of a slope generates an upslope flow, and the vorticity of this flow is countered by the baroclinic generation of vorticity (baroclinic torque) that facilitates flow separation (Crook & Tucker 2005). Thus, the separation is governed by two opposing vorticities, a concept that was used as the basis of a simple theoretical model developed in that paper to predict the separation of an upslope flow over a uniformly heated simple slope in the absence of background mean flow.

The present study was motivated by field experiments that were conducted at the Granite Mountain atmospheric sciences test bed (GMAST) of the US Army Dugway Proving Ground, Utah, under the mountain terrain atmospheric modelling and observations (MATERHORN) program (Fernando & Pardyjak 2013; Fernando *et al.* 2015). During this extensive field study, selected measurement equipment was repositioned for a limited period to observe flow separation from a wide slope as well as associated cumulus cloud formation aloft. The flow separation/cumulus formation was evident under quiescent background conditions dominated by high pressure. The positioning of a Doppler wind LiDAR to detect flow separation was problematic, given the logistical challenges of access to the slope and supplying power to the LiDAR site. The availability of guidance from a controlled study and a model to predict the separation distance were perceived as particularly helpful in field experimental planning. To this end, a laboratory experiment was conducted by heating a uniform slope (a planar incline) with a constant heat flux to generate an upslope flow, and the flow separation on the slope was observed as a function of a wide range of external parameters. Extensive measurements of the velocity field and separation length were made, steered by which a simple theoretical model was developed to explain the observations. The results were extrapolated to the MATERHORN field experimental case. Overall, the results are expected to help plan and interpret field observations, develop parameterizations and provide validation data for numerical modelers.

2. Previous related work

Since the epochal review of Queney (1948) on flow over low and steep hills, the progress of mountain meteorology has been remarkable (Taylor & Teunissen 1987;

https://doi.org/10.1017/jfm.2015.298 Published online by Cambridge University Press

Blumen 1990; Scorer 1997; Whiteman 2000). Significant progress has been made on mean flow (synoptic flow driven by large-scale pressure gradients) approaching mountains, especially for neutral (Belcher & Hunt 1998) and stably stratified cases (Baines & Manins 1989; Baines 1995; Boyer & Davies 2000). For the neutrally stratified case, the pioneering two-dimensional (2D) linear analysis of Jackson & Hunt (1975) considered low hills with small slopes, say $<10°$ (Hewer 1998). The analysis has been extended to three-dimensional (3D) cases of practical relevance (Mason & King 1985; Hunt, Leibovich & Richards 1988; Carruthers *et al.* 2012), and the flow features of 2D and 3D cases have been shown to differ substantially (Doyle & Durran 2007). For steeper slopes without ground heating, the flow separation and a recirculation bubble may appear in the lee of the slope. Weakly (Xu, Ayotte & Taylor 1994) and full (Apsley & Castro 1997; Crook & Tucker 2005) nonlinear models have been developed for flow past idealized topographies, models for flow separation have been developed for non-stratified flows (Lighthill 1963), and estimates have been made for the critical slope for flow separation (Wood 1995). A number of numerical, field observational and wind tunnel studies on flow separation in neutral flows over topography have been reported (Britter, Hunt & Richards 1981; Gong & Ibbetson 1989; also see, Mason & King 1985; Hunt 1991 and Hewer 1998).

The inclusion of thermal forcing may drastically change the flow character, depending on the competition between ensuing thermal circulation (up/downslope and up/down valley flows) and external flow. A few theoretical studies have been reported in this regard, for both 2D (Raymond 1972; Smith & Lin 1982; Tian & Parker 2003) and 3D (Reisner & Smolarkiewicz 1994) cases. Using scaling arguments, Mason (1987) derived a form of Froude number that helps delineate convective versus external flow dominated cases, which has broad consistency with that proposed by Lewis *et al.* (2008). Numerical studies with periodic 2D hills show that, for low hills, convective flow structures that develop without the external flow are similar to those which appear on flat terrain, but the presence of even a weak mean flow modifies them. When an external mean flow is present, both transverse and longitudinal rolls develop, in contrast to the longitudinal rolls that appear without the mean flow (Dörnbrack & Schumann 1993; also see Krettenauer & Schumann 1989). According to the 2D simulations of Dörnbrack & Schumann (1993), an external flow (with velocity $\overline{U}$) may impact on convective structures for $\overline{U}/w_* > 2$, where $w_* = (g\alpha\overline{w'T'}h)^{1/3}$ is the convective velocity, g gravity, α the thermal expansion coefficient, $\overline{w'T'}$ the vertical temperature flux at the surface and h the mean height of the flow, whence the influence of topographic details wanes in determining turbulent statistics of the overlying flow. The cause of the waning is the mean flow which tends to destroy any coherent roll motions induced by the undulating terrain for zero mean flow and therefore reduces the impact of the terrain parameters on the turbulence statistics. They showed that, for low hills of sufficient steepness, heating reduces the likelihood of lee-side flow separation, and the characteristic size and velocity of the separation bubble are reduced when heating is present. This is due to the enhanced vertical momentum diffusion on the windward side of the mountain due to convection, thus reducing the vorticity of the leeward separation bubble (Allen & Brown 2006). On the other hand, for steeper and high topographic features, heating facilitates the lee-side flow separation, and for a given flow velocity and valley width, the separation occurs above a critical heating rate. Lehner & Whiteman (2012) have studied separation features of idealized basin-shaped topographies using a large-eddy simulation (LES) version the Weather Research and Forecasting (WRF) model. They employed spatial

https://doi.org/10.1017/jfm.2015.298 Published online by Cambridge University Press

and temporally varying heating, and noted that thermal asymmetry so introduced leads to closed circulations cells that move toward sidewalls of more pronounced heating.

Crook & Tucker (2005) demonstrated that flow past a uniformly heated topography, consisting of an obstacle above a flat surface, can be approximated by flow past the topography with heating occurring over the obstacle surface only. They developed linear and nonlinear models and, in the former, flow past a heated low hill could be analysed by superposing the separate responses of thermal and orographic forcing. To our knowledge, no laboratory experiments delving into flow separation in heated mountainous terrain have been reported hitherto, although a number of studies have dealt with flow over a heated uniform slope (Chen *et al.* 1996) and complex topography with spatially varying slopes (Berman *et al.* 1995; Reuten *et al.* 2007) in the presence of background stable stratification. The stable stratification appears to have a tendency to suppress flow separation, and this case is relevant to the morning transition in complex terrain during which the nocturnal inversion is destroyed by heating of the ground during sunrise (Lu & Turco 1994; Princevac & Fernando 2008). The present paper considers the case without background stratification, which mimics the case of upslope flow after the morning transition.

3. Experiments

The experiments were carried out in a glass tank of rectangular cross-section (125 cm × 30 cm) filled with deionized water to a depth of 30 cm. To minimize heat leakage to ambient air, water at the room temperature was used, and 5 cm thick styrofoam thermal insulation encased the tank on all sides. The top insulation isolates the tank from ambient air, thus ensuring two-dimensionality of the flow and absence of secondary circulation. A removable window in the insulation allowed optical access to the flow. A unit serving as a 15.6 cm × 30 cm heated slope was custom manufactured, which consisted of an array of densely packed heating wires embedded in silicon rubber. The bottom of the pad was fully insulated. The unit was heated by applying a constant DC current and could attain a maximum possible heat flux of 2.0 kW m^{-2}, where the heat flux could be estimated as $Q = IV/A$, where I is the applied current, V the applied voltage and A the slope area. This estimation was independently verified using the standard calibration techniques described in Hunt, Fernando & Princevac (2003).

Two experimental configurations were considered, as sketched in figure 1. In the first, the slope was placed abutting the wall (figure 1*a*), and by assuming that the no-slip condition plays a lesser role in the overall plume dynamics, the flow was considered similar to the case of a symmetric triangular-shaped mountain (figure 1*b*). This assumption is particularly plausible for thicker (vertical) plumes, whence the flow separation is unaffected by the vertical wall. A series of experiments was conducted using both configurations, under otherwise identical conditions, and the separation points observed were within ±5 % with no particular bias for one case or another. Given that the configuration in figure 1(*a*) allows longer flow development times before the endwalls become important, the majority of the experiments were conducted using that configuration.

In the experiments, the water tank was allowed to settle for two hours for residual motion to decay, whereupon a prescribed current was applied to the heating elements. Video recordings were made of the initial transients, the quasi-steady current feeding the upslope flow and the flow separation. The experiment was terminated when

https://doi.org/10.1017/jfm.2015.298 Published online by Cambridge University Press

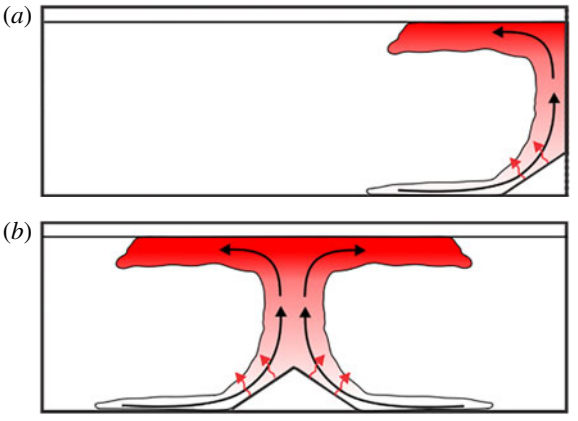


FIGURE 1. (Colour online) Schematics of experimental configurations used.

measurable velocities were detected at the distant endwall. Post-processing of the data allowed identification of a quasi-steady period. The temperature of the sloping surface was obtained using a number of k-type thermocouples. Eleven prescribed slope angles $\beta = 0°$, $5°$, $10°$, $15°$, $18°$, $20°$, $25°$, $30°$, $35°$, $40°$ and $45°$ were used, and the heat flux was varied between 9.4 W m^{-2} and 2.0 kW m^{-2}.

Flow velocities were measured using particle tracking velocimetry (PTV). The flow was seeded with orange fluorescent polyethylene particles, 90 μm in diameter and density $\rho \approx 1$ g cm^{-3}. A 3 mm thick Ar-ion laser sheet (wavelength $\sim$ 510 nm), introduced through a vertical slit in the insulation, provided illumination for a vertical cross-section of the flow in the middle of the tank. The spheres are sensitive to a wide range of excitation wavelengths and emit light at $\sim$600 nm. The particle motions were viewed through an orange filter of cutoff wavelength $\sim$600 nm to achieve high-contrast images with easy particle detection and processing, while eliminating light from sources other than moving particles. To obtain optimal particle track detection, special attention was paid to ensuring sufficient water clarity and particle seeding density. A 752 pixel $\times$ 480 pixel CCD camera positioned in front of the observation window was used to record videos of particle motion at 5 f.p.s. The camera was set to capture the flow at the slope and its immediate vicinity at 35–54 pixel cm^{-1} spatial resolution. Recorded videos were split into individual frames and processed by in-house-developed PTV software. Image enhancement was first applied to improve the contrast as well as for spatial filtering. Individual particles were then detected in each frame, allowing reconstruction of 2D particle motions. In later stages of data processing, the velocity components were calculated using track information.

To confirm that the insulation was sufficient, numerous vertical and horizontal cross-sections of the flow were imaged and analysed using PTV for experiments with different slope angles. The horizontal flow in the far field, especially in the central region of the tank, and its modification when approaching the near field of the slope were interrogated. Particle tracks and velocity components allowed detection of the distance L_s along the slope at which the flow separates as well as calculation of the mean local velocity U_s at the separation point.

The distance L_s was detected by examining a map of particle tracks and with the help of feature tracking visualizations (FTV). The latter reconstructed particle paths

https://doi.org/10.1017/jfm.2015.298 Published online by Cambridge University Press

by colour mapping them according to the track length and/or velocity, thus providing a good representation of the time history of the flow. A combination of static paths maps and FTV animations allowed confident detection of L_s with acceptable accuracy, which is discussed further in § 6.1. The values of U_s were then obtained by ensemble-averaging velocities in the vicinity of the separation point. Wherever possible, the uncertainties were estimated using the technique of Kline & McClintock (1953).

4. Experimental observations

Observations were made from the initiation of heating until the plume recirculation flow reached the opposite tank wall. At first, small-scale roll structures appeared on the slope that broke down to form an upslope flow that separated, rose vertically, deflected from the top surface and flowed horizontally as an intrusion (figure 1). This transition period lasted for up to 200 s, but it varied with the experimental parameters, i.e. the higher the buoyancy flux, the shorter the transient period. As the plume intrusion gradually propagated into the tank interior, the upslope flow and the plume generated by its separation underwent a quasi-steady period. During this period, the upslope flow, rising plume and the resulting intrusion developed without any apparent influence of the endwalls. When the endwall influence sets in, a large quasi-stationary cell developed in the tank that clearly affected flow in the tank, including the upslope flow. All phases of flow evolution were observed by PTV-track maps constructed from intervals of 250 images (50 s based on 5 f.p.s.); see figure 2. Reuten *et al.* (2005) hypothesized that a recirculating flow may develop surrounding the upslope flow, thus trapping fluid parcels in a cell above the slope. Such closed-loop circulation was not observed in the present case; instead the upslope flow was fed by the lateral entrainment. The slope flow separated at a distance L_s from the mountain foot, and lofted the buoyant fluid.

Figure 2(*b*) shows PTV pathlines obtained in the plan view by illuminating a horizontal cross-section at a representative height of 4 cm above the bottom (figure 2*a*). The corresponding vertical cross-section through the centre of the tank is given in figure 2(*c*). Observations at several other horizontal planes also exhibited similar characteristics (not shown). Note the 2D nature of the flow, except near the tank walls where some deviations could be seen (figure 2*b*). Given the 2D nature, particles could be tracked throughout the field of view, providing long pathlines. Of course, two-dimensionality is less evident near the slope, where the flow is complicated by turbulent upslope flow, separation and plume formation.

An interesting observation was the response of slope flow to varying slope angle β. When $\beta > \beta_c$ ($\approx 20°$), the flow consisted of upslope flow at low elevations, flow separation at L_s, and a rising plume fed by the separated upslope flow (figure 3*a*). Up to some vertical distance from the location of formation (i.e. region of flow separation), the plume is mainly driven by the buoyancy of fluid parcels, aided by the initial vertical momentum of fluid parcels that arise from the antecedent upslope flow. The rising plume away from the source region is fed by fluid entraining from the surroundings, which approaches the rising plume almost horizontally.

It is well known that when a buoyant fluid with some initial vertical momentum is released, the incipient motion is momentum dominated (as in the case of a jet), and after rising to the momentum length L_M the motion becomes buoyancy dominated (behaves as a plume); see List (1982) and Papanicolaou & List (1988). For the present 2D case, the momentum length scale becomes $L_M = M_0/B_0^{2/3}$, where the plume source following flow separation has a total vertical kinematic momentum flux

https://doi.org/10.1017/jfm.2015.298 Published online by Cambridge University Press

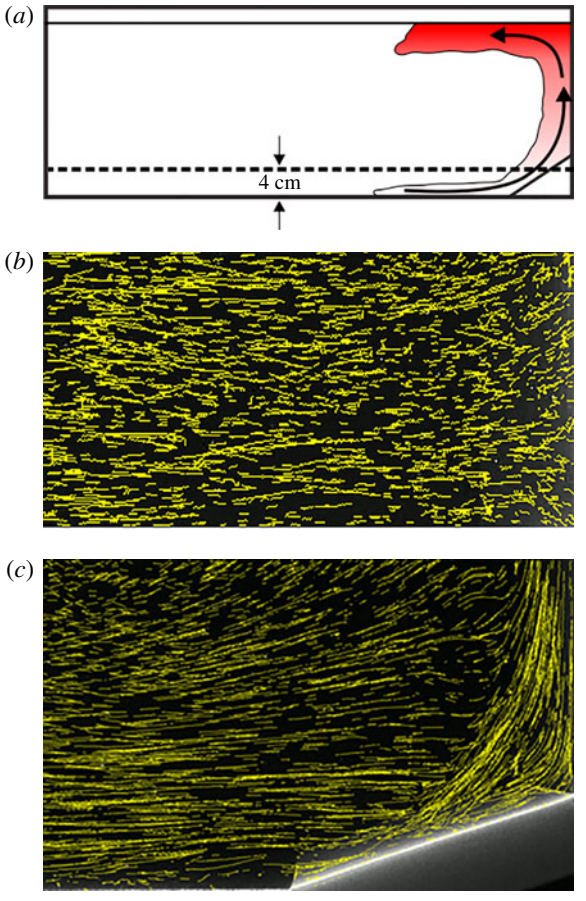


FIGURE 2. (Colour online) Particle tracks at an illuminated cross-section, which shows an approach flow, parallel to the walls ($\beta = 20°$). The dashed line in (*a*) is the location of (*b*), the horizontal cross-section 4 cm above the bottom. (*c*) The vertical cross-section passing through the tank centre in its long direction.

per unit width M_0 and a buoyancy flux B_0 (also see § 5). Typical values of L_M for the present experiments are on the order of 4 cm.

As β decreases, the separation point recedes, arriving at a scenario where the upslope flow is not sufficiently developed to supply fluid to the separated plume, as shown in figure 3(*b*). This appears at $\beta \leqslant \beta_c$ (figure 3*b*), and appreciable entrainment of outside flow into the core of the plume could be observed at the level of plume formation, together with the increasing 3D nature of the flow. Further reduction of β completely eliminated the upslope flow, which was observed when $\beta \leqslant 10°$, whereupon the flow is much like a plume from a horizontal source of finite dimensions; see figure 3(*c*). Note that, in the near field, 2D plumes of finite width are different from those of zero width (line plumes). Colomer, Boubnov & Fernando (1999) have studied the former for the axisymmetric case and Rouse, Yih & Humphreys (1952) reported a comprehensive study on the latter. The development of a simple theoretical model followed the experimental observations and is described next.

https://doi.org/10.1017/jfm.2015.298 Published online by Cambridge University Press

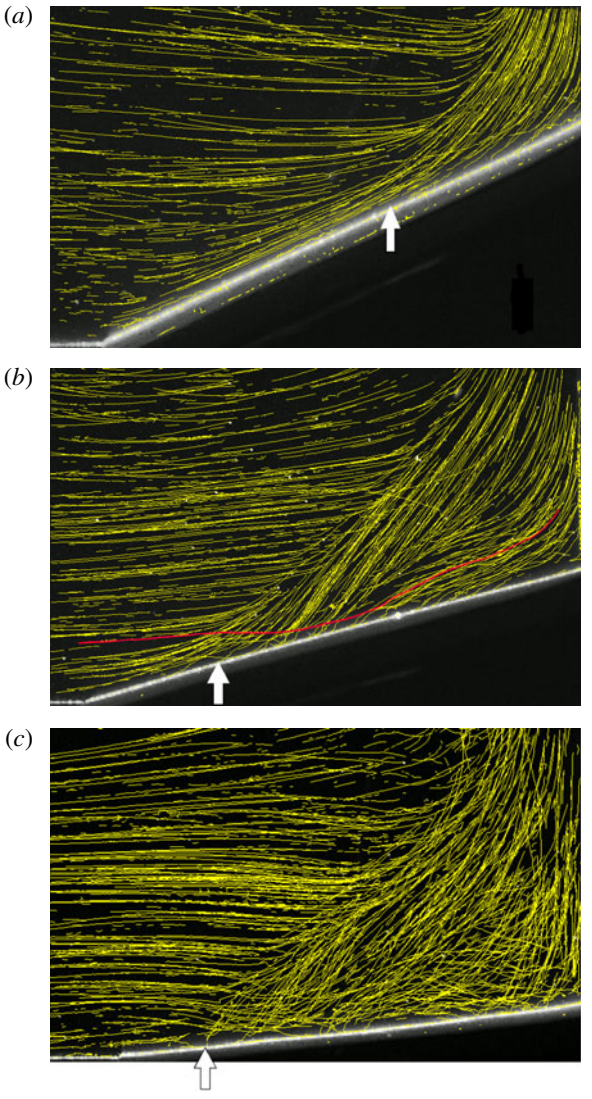


FIGURE 3. A track map extracted from an FTV animation. It illustrates the long-exposure pathlines of fluid parcels: (*a*) $\beta = 25°$, (*b*) $\beta = 15°$, (*c*) $\beta = 5°$. The white arrow represents the estimated separation point. Note that in (*a*) very few outside parcels penetrate the plume core, causing upslope flow to feed the plume entirely, whereas in (*b*,*c*) there is substantial penetration as illustrated by the red particle track in (*b*).

5. Model

Consider a 2D upslope flow that develops on a uniformly heated incline of length L_0 and of slope angle β described by along-slope (s), slope-normal (n) and y coordinates as shown in figure 4. The ambient fluid is neutrally stratified, approximately mimicking quiescent atmospheric cases after the breakup of inversions (Pardyjak *et al.* 2009). The flow starts developing at the base of the incline as an upslope flow, entraining fluid from the surroundings. As the flow develops along the slope with upslope velocity u in the s direction, the heating of the incline amplifies

https://doi.org/10.1017/jfm.2015.298 Published online by Cambridge University Press

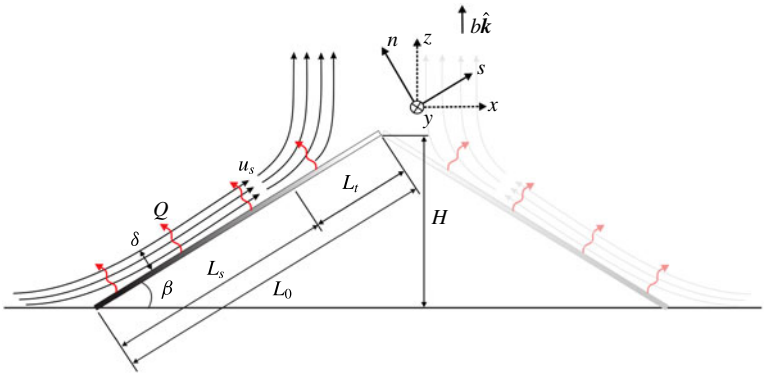


FIGURE 4. (Colour online) A schematic of the upslope flow. At the flow separation, the flow rises as a plume that is fed by the anabatic flow.

the baroclinic torque ($\nabla \times b\hat{\boldsymbol{k}}$) that counters the vorticity advection by the shear flow ($\boldsymbol{u} \cdot \nabla \boldsymbol{\omega}$), thus facilitating the flow separation. These competing terms appear in the vorticity ($\boldsymbol{\omega}$) equation (to the Boussinesq approximation) as

$$\frac{\partial \boldsymbol{\omega}}{\partial t} + \boldsymbol{u} \cdot \nabla \boldsymbol{\omega} = \boldsymbol{\omega} \cdot \nabla \boldsymbol{u} + \nabla \times (b\hat{\boldsymbol{k}}) + \nu \nabla^2 \boldsymbol{\omega}, \tag{5.1}$$

where ν is the viscosity, $\boldsymbol{u}$ the velocity, b the buoyancy $b = g(\rho_0 - \rho)/\rho_0$, ρ the density, ρ_0 a reference density, g gravity and t the time. The y component of vorticity ω_y becomes

$$\frac{\partial \omega_y}{\partial t} = (\nabla \times b\hat{\boldsymbol{k}})_y - u\frac{\partial \omega_y}{\partial s}. \tag{5.2}$$

Assuming Reynolds number similarity, the viscous influence can be neglected. At the separation point the opposing vorticities balance, and $u\partial\omega_y/\partial s \sim (\nabla \times b\hat{\boldsymbol{k}})_y$, with $(\nabla \times b\hat{\boldsymbol{k}})_y = -\partial(b\cos\beta)/\partial s$. Using the scaling $u \sim U$, $b \sim \Delta b$, $\omega_y \sim \omega$, $\partial/\partial n \sim 1/\delta$ and $\partial/\partial s \sim 1/s$, where δ is the upslope-layer thickness (that grows along the slope), the vorticity scaling at separation becomes $\omega_y \sim \Delta b \cos\beta/U$. At the separation point, ω_y generated by buoyancy is balanced by that due to boundary-layer shear, $\omega_y = \partial u/\partial n \sim U/\delta$. Using subscript s to denote the separation point, the condition for the upslope flow separation can be written as $\omega_s \sim \Delta b_s \cos\beta/U_s \sim U_s/\delta_s$ or

$$U_s^2 \sim \Delta b_s \cos\beta \delta_s. \tag{5.3}$$

Using the approximate buoyancy conservation equation, $\partial(bu\delta)/\partial s \approx q_0$, where $q_0 = g\alpha Q/\rho_0 C_p$, Q the heat flux per unit area and C_p the specific heat (Schumann 1989), an additional scaling equation is possible,

$$\Delta b_s U_s \delta_s \sim q_0 L_s, \tag{5.4}$$

where L_s is the separation length. From (5.3) and (5.4), the upslope velocity at the flow separation becomes

$$U_s \sim (q_0 L_s \cos\beta)^{1/3}. \tag{5.5}$$

A velocity scale for upslope flows has been derived by Hunt *et al.* (2003), by considering a steady turbulent shear flow generated by heating an incline. Their

https://doi.org/10.1017/jfm.2015.298 Published online by Cambridge University Press

model consisted of several layers with disparate dynamics, each having an intrinsic transport mechanism. The velocity scale so derived, $U \sim (q_0\delta \sin\beta)^{1/3}$, is expected to be valid up to flow separation. Equating the two estimates at the separation point, we get $L_s/\delta_s \sim \tan\beta$. Field and laboratory observations show that the separated flow rises as a plume formed in the region between the separation point and the apex of the slope (see § 6.3), for example, as shown in figures 2–4. The volume flux of the plume is mainly fed by the anterior anabatic flow (e.g. Geerts, Miao & Demko 2008), as was evident from the present experiments at higher slopes $\beta > \beta_c$. The total buoyancy flux fed into the plume is $B_0 = q_0 L_t$, where $L_t = L_0 - L_s$, and the buoyancy flux over an equivalent horizontal plane is

$$q_0^* = \left(\frac{q_0 L_t}{L_t \cos\beta}\right), \tag{5.6}$$

where we have assumed that the effect of the total buoyancy flux emanating from the slope is equivalent to that of a horizontal source with the same total buoyancy flux distributed uniformly. The buoyancy (b), vertical velocity (w), and near-field entrainment velocity (u_e) scaling for horizontal plume sources of finite dimensions (L_w) driven by a buoyancy flux (q_0^*) has been proposed by Colomer *et al.* (1999), which is a variant of the well-known scaling for point and line plumes (List 1982). For 2D horizontal sources of finite source dimensions, the analogous 2D near-field scaling can be readily written as

$$b \sim \frac{(q_0^* L_w)^{2/3}}{L_w}, \quad w \sim (q_0^* L_w)^{1/3} \quad \text{and} \quad u_e \sim (q_0^* L_w)^{1/3}. \tag{5.7a–c}$$

The vertical plume velocity in the proximity of the finite-width source generated by flow separation now becomes $w_s \sim (q_0^* L_t \cos\beta)^{1/3}$, where the source half-width of the 2D plume is $L_w = L_t \cos\beta$. Using (5.6) and (5.7), the vertical plume velocity scale can be written as $w_s \sim (q_0 L_t)^{1/3}$.

As discussed in § 4, when there is initial momentum to the buoyant fluid, the rising flow is transformed into a true buoyant plume after a vertical distance of $L_M = M_0/B_0^{2/3}$, and for the present case $M_0 \approx U_s^2 \delta_s \sin\beta$, $B_0 \approx q_0 L_t$ and thus $L_M \sim L_s (L_s/L_t)^{2/3} \cos^{4/3}\beta$. Note that (5.7) is strictly valid beyond L_M (which is suitably small in our cases), and hence in comparing with (5.7), the velocity measurements need to be taken at an appropriate distance from the flow separation location.

It is assumed that for $\beta > \beta_c$ the total vertical volume flux of the plume at the separation location $\sim (q_0 L_t)^{1/3} L_t \cos\beta$ is balanced by the along-slope volume flux of the anabatic flow $\sim U_s \delta_s$ that feeds the plume. Equating the two fluxes at the point of separation, $U_s \delta_s \sim (q_0 L_t)^{1/3} L_t \cos\beta$ and using (5.5) and $L_s + L_t = L_0$, an expression for L_s/L_0 is obtained,

$$\frac{L_s}{L_0} = \left[1 + \Pi \frac{\sin^{1/4} 2\beta}{\sin\beta}\right]^{-1}, \tag{5.8}$$

where Π is a proportionality constant arising from the scaling. From (5.8), it is evident that L_s/L_0 has a weaker dependence on β at large β. Also note that (5.8) is a definitive form of the functional relationship obtained from straightforward dimensional analysis, $L_s = f(q_0, L_0, \beta, \nu)$. With $\beta = \beta(L_0, H)$, where H is the summit height,

$$\frac{L_s}{L_0} = f_1\left(\frac{H}{L_0}, Re_H\right) \to f_2\left(\frac{H}{L_0}\right) = f_2(\beta), \tag{5.9}$$

https://doi.org/10.1017/jfm.2015.298 Published online by Cambridge University Press

for large $Re_H = (q_0 H)^{1/3} H/\nu$, where f_1 and f_2 are functions. Note that Re_H is an implicit form of the Reynolds number. At large Re_H the Reynolds number similarity follows, hence causing f_1 to be independent of Re_H. Since Re_H is defined in terms of bulk parameters, it does not explicitly represent the velocity and length scales or slope angle dependence. Alternatively, a Reynolds number Re_U can be defined in terms of the scales at flow separation, i.e. $Re_U = U_s \delta_s/\nu$, which is related to Re_H.

Recall that the above formulation is valid for $\beta > \beta_c$, and in § 4 it was pointed out that in the limit $\beta \to 0$ the flow approaches that of a uniformly heated horizontal plume source of finite width ($L_w \approx L_0$), where scaling (5.7) is applicable. In this regime the slope is sufficiently small (or below a critical slope β_u) to suppress the upslope flow. According to the measurements and theoretical arguments of Princevac & Fernando (2007), for a given fluid, $\beta_u(Pr)$ is fixed, being dependent only on the Prandtl number Pr for the case of upslope flows starting from rest.

As discussed by Colomer *et al.* (1999), a plume of finite width recedes toward its centre from the edge of the source. This is nominally a flow separation region occurring due to horizontal entrainment flow into the plume that overshadows rising thermals at its edge (figure 3*c*). The characteristic lateral penetration (or separation) distance L_s of the entrainment flow before the liftoff can be estimated using the vertical momentum equation, by considering a balance of buoyancy forces due to heating of the entrainment flow and the vertical inertia forces, viz.

$$b \sim \frac{\mathrm{D}w}{\mathrm{D}t} \sim u\frac{\partial w}{\partial x} \sim \frac{u_e w}{L_s} \sim \frac{\alpha_1 w^2}{L_s}, \tag{5.10}$$

where L_s is the separation distance from the edge, w the vertical velocity outside the thermal boundary layer, $u_e = \alpha_1 w$ the entrainment velocity, and α_1 the entrainment coefficient for 2D plumes (according to Rouse *et al.* 1952, for 2D line-source plumes, $\alpha_1 \approx 0.25$). Note that this estimation is valid above the boundary-layer region of entrainment flow arriving at the heated surface. Together, (5.10) and (5.7) give

$$L_s \sim \alpha_1 L_0. \tag{5.11}$$

The detailed predictions made in this section are evaluated against experimental data in § 6.

6. Experimental measurements

6.1. *Separation length*

To obtain a quasi-steady flow with minimum endwall influence for a reasonable period, a particular range of buoyancy fluxes q_0 was necessary, and our study focused only on such cases. For q_0 below this range, the flow either developed eddies that rolled up the slope (similar to laminar convection on slopes; Chen *et al.* 1991) or circulated in a counterclockwise direction as a single stationary eddy of size approximately equal to the depth of the tank. When conditions for quasi-steady upslope flow prevailed, the mean flow was slope-parallel, with entrainment at its edges, and flow separation occurred at a distance L_s from the bottom (figure 3*a*). Small fluctuations in the separating flow paths were detected, confirmed by releasing small amounts of fluorescent dye on the slope and by FTV animations.

The distance to the separation point L_s was detected for each of the examined cases, and was determined by manually examining particle tracks obtained from PTV and

https://doi.org/10.1017/jfm.2015.298 Published online by Cambridge University Press

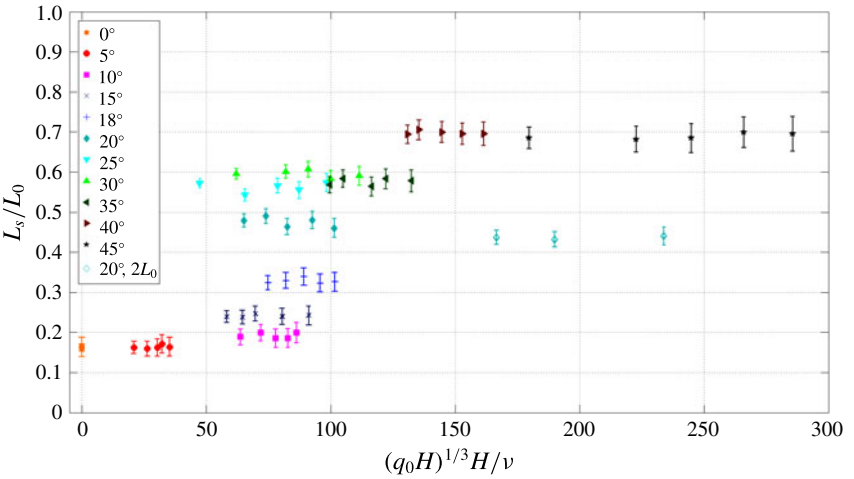


FIGURE 5. (Colour online) Dimensionless flow separation distance L_s/L_0 as a function of Re_H. The calculation of error bars is given in § 6.1. The ◇ symbols show the double slope configuration data (figure 1*b*).

selecting the point of the first visible track separation from the slope. The detected separation point location was then verified, and corrected if necessary, by examination of FTV animations. A combination of both the static map of particle tracks and FTV animations provided an accurate detection of L_s. The position error was estimated to be less than the distance travelled by a particle during three consecutive frames, $\Delta L_s = \pm 3\Delta t U_s$, where Δt is the time delay between the frames, based on the image acquisition frame rate of 5 f.p.s.

Figure 5 shows the dimensionless separation distance L_s/L_0 as a function of $Re_H = (q_0H)^{1/3}H/\nu$ for all of the examined slope angles β. A reasonable parameter range could be obtained by varying the buoyancy flux q_0. The estimated errors of L_s/L_0 were $\sim$10 % for lower Re_H and less than 3 % for higher Re_H, and are presented as error bars. The separation distance increased with the slope angle, from $0.16L_0$ for 5° and up to $0.7L_0$ for the largest examined angle of 45°. With the decrease of β, a higher q_0 was required to initiate the upslope flow. The results show that, at each angle, the separation distance is virtually a constant and therefore is Re_H independent at all ranges of Re_H. This confirms the Reynolds number similarity assumption made in (5.2).

Next, a double slope configuration was used, as in figure 1(*b*), with each slope having a length of 15.6 cm. The measurements were performed at slope angles of 20° and 30°, resulting in similar L_s/L_0 values (within ±5 %) to those presented in figure 5; the corresponding data points for $\beta = 20°$ are included in figure 5. The double slope, however, increased the rising flux of buoyant fluid above the slope, causing the rapid formation of a thick, warm layer at the top, which violated the assumption of constant background density. Therefore, results from the double slope were limited to a few cases.

The measured normalized separation lengths are shown in figure 6 as a function of β, together with the prediction (5.8). The model and the data agreed well for $\beta > 20°$, with $\Pi = 0.35$ but below the critical inclination $\beta_c \approx 20°$, the model overpredicted the separation length. The data show a sharp drop of L_s/L_0 for $20° \geqslant \beta > 10°$ and an

https://doi.org/10.1017/jfm.2015.298 Published online by Cambridge University Press

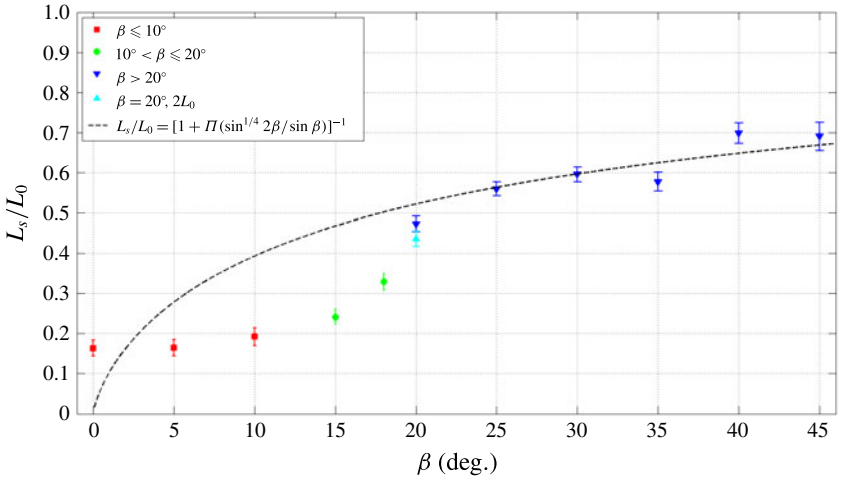


FIGURE 6. (Colour online) Ensemble-averaged dimensionless separation length L_s/L_0 as a function of the slope angle β. The dashed line represents the separation length prediction (5.8) with $\Pi = 0.35$.

approximately constant $L_s/L_0 \approx 0.2$ for $\beta \leqslant 10°$. Based on the observations discussed in § 4, this can be attributed to the transition from a flow where the upslope flow supplies the entire volume flow of the separated plume ($\beta > \beta_c$) to one where the source region of the separated plume draws volume flux from both the upslope flow and background ($\beta \leqslant \beta_c$). The weak variation of L_s/L_0 with β for $\beta \leqslant 10°$ can be construed as due to the approach of the horizontal-plume regime, as discussed in § 4. In this case, the contribution of the upslope flow is unimportant and the plume rises from almost the entire slope length. The estimation (5.11) for this case, $L_s \sim \alpha_1 L_0$, is in good agreement with the observations of figure 6 that show $L_s/L_0 \approx 0.16$ for $\beta \leqslant 10°$. This is consistent with entrainment coefficients α_1 for horizontal line plumes ($\alpha_1 \approx 0.25$), yielding an $O(1)$ proportionality constant of 0.65 for (5.11).

As stated in § 5, the formation of upslope flow on an inclined heated slope is possible when $\beta > \beta_u(Pr)$, and for the present work, based on the model of Princevac & Fernando (2007), $\beta_u \approx 5°$. This is broadly consistent with the observation that the pure plume regime is originated for $\beta \leqslant 10°$, taking into account that Princevac & Fernando (2007) considered the (transient) case of initial upslope flow formation from rest and the present work deals with plumes at the steady state. Also note the narrow regions of figure 6 where constant L_s/L_0 can be identified even for $\beta > \beta_c$. In such regions, we have not been able to observe any mechanistic changes to the flow or systematic departure of data from the model. Therefore, we have not placed an emphasis on such observations.

6.2. *Velocity magnitude*

A small rectangular region of interrogation (± 0.4 cm) around the detected point of separation was chosen to obtain the local mean velocity magnitude at the point of separation U_s. To ensure the full inclusion of the near-slope boundary layer, the rectangle included a portion of the slope itself, resulting in a partial combination of raw velocity data with some falsely detected values. Particle velocities were calculated in this region by dividing digitized track lengths between two consecutive frames by

https://doi.org/10.1017/jfm.2015.298 Published online by Cambridge University Press

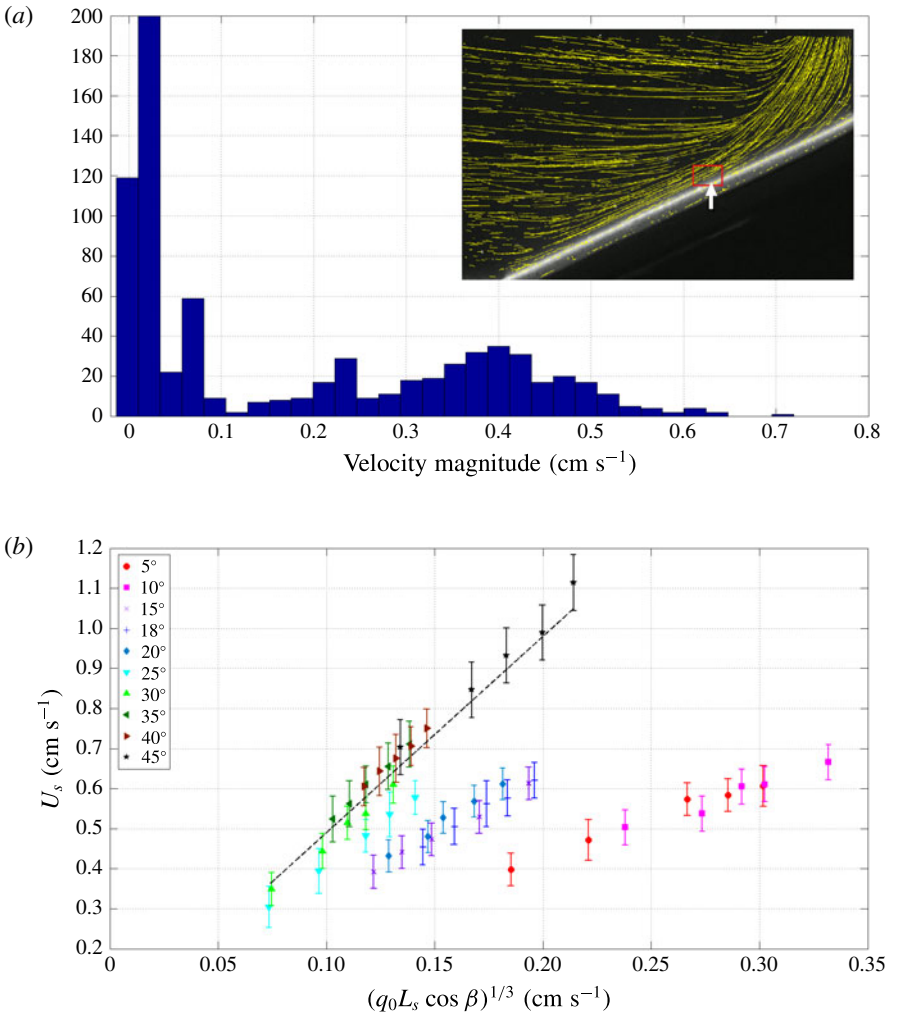


FIGURE 7. (Colour online) (*a*) Velocity magnitude distribution histogram at the point of separation. Inset figure shows an example of the small region of interest that was chosen in the vicinity of the point of separation ($\beta = 20°$). (*b*) Local mean upslope velocity, U_s, at the point of flow separation. Dashed line is a linear fit (5.5) with the proportionality constant $\gamma = U_s/(q_0 L_s \cos\beta)^{1/3} = 4.9$. The calculation of error bars is given in § 6.2.

the frame rate value (5 f.p.s.). A representative histogram of calculated velocity magnitudes is shown in figure 7(*a*).

The main ensemble of velocity magnitudes was distributed in an approximate bell shape, close to a normal distribution, as seen in the histogram. The velocity values on either extreme of the distribution were filtered out from the ensemble; they were attributed to false particle detection at the slope surface caused by the laser sheet reflection and particles outside the separation region. This filtering method allowed an accurate measurement of the velocity; based on the particle position detection accuracy of ± 0.5 pixels, spatial resolution 35–54 pixel cm^{-1} and a frame rate of 5 f.p.s., errors are estimated to be from 6.8 % to 10 %.

https://doi.org/10.1017/jfm.2015.298 Published online by Cambridge University Press

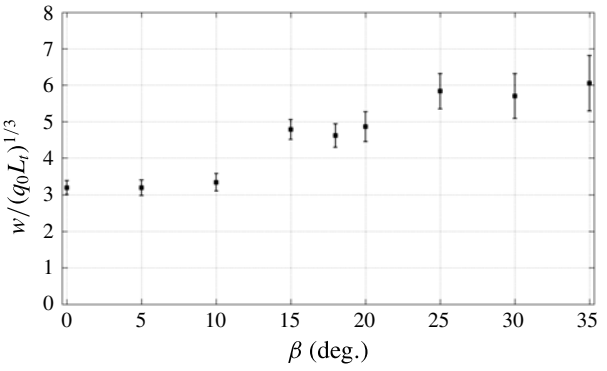


FIGURE 8. Ensemble-averaged dimensionless vertical velocity, $w/(q_0L_t)^{1/3}$, of the plume at $z = 0.3L_t \cos\beta$ above the slope apex as a function of β. Here w is the plume velocity outside the thermal boundary layer and $L_t \cos\beta$ is the plume half-width. Data beyond the 35° angle were unusable, because the field of PTV visualization did not capture a reasonable area near the plume source.

In the analysis, interestingly, the along-slope velocities at the separation point U_s were found to fall into three distinct regimes, consistent with those identified in § 4. All data for $\beta > \beta_c$ ($\approx 20°$) followed (5.5), with a proportionality constant of 4.9, as shown in figure 7(*b*) as a plot of U_s versus $(q_0L_s \cos\beta)^{1/3}$. The data at $\beta = 25°$ show some deviation from the data cluster of $\beta > 20°$, perhaps indicating a gradual move toward a different dynamical regime that onsets between $\beta = 20°$ and 25°. The deviation, however, remains within the error bars and hence definite conclusions could not be made on the departure. Also evident is the clustering of data for $15° \leqslant \beta \leqslant 20°$, which is the transition regime wherein the separated plume could not be supplied only via the upslope flow. Results for $\beta \leqslant 10°$ also showed a distinct cluster, arguably approaching the case of plumes from horizontal sources of finite size (figure 3*c*). The data therein follow (5.7), with U_s being the lateral entrainment flow, $U_s \sim (q_0L_s \cos\beta)^{1/3} \approx (q_0L_0)^{1/3}$ for small β. This is also equivalent to $U_s \sim (q_0L_s \cos\beta)^{1/3}$, which is supported by figure 7(*b*), given that $L_s \sim L_0$.

To further corroborate the velocity scaling for plumes after flow separation, the ensemble-averaged dimensionless vertical velocity (following from figure 7), $w/(q_0L_t)^{1/3}$, of the plume versus β is shown in figure 8. These measurements were taken at a distance $z = z_m = 0.3L_t \cos\beta$ above the slope apex, where $L_t \cos\beta$ is the plume half-width. The selection of z_m followed the inferences of Colomer *et al.* (1999) that it is within the near field of the plume source where (5.7) holds and that it approximately satisfies the momentum length scale L_M criterion of § 5 ($L_M \sim 4$ cm). For $\beta \leqslant 10°$, $L_t \approx 0.8L_0$, the flow behaves as a plume of finite diameter and w scales as (5.7). In $10° < \beta \leqslant 20°$, the flow is in a transition regime and with increasing β the flow approaches another regime with $w/(q_0L_t)^{1/3} \approx 6$, supporting the underlying arguments of the model developed in § 5.

6.3. *Field measurements*

The field experiments were conducted at the GMAST of the US Army Dugway Proving Ground, Utah, as a component of the MATERHORN Program (for details see Fernando & Pardyjak 2013). GMAST is centred around a single isolated (Granite)

https://doi.org/10.1017/jfm.2015.298 Published online by Cambridge University Press

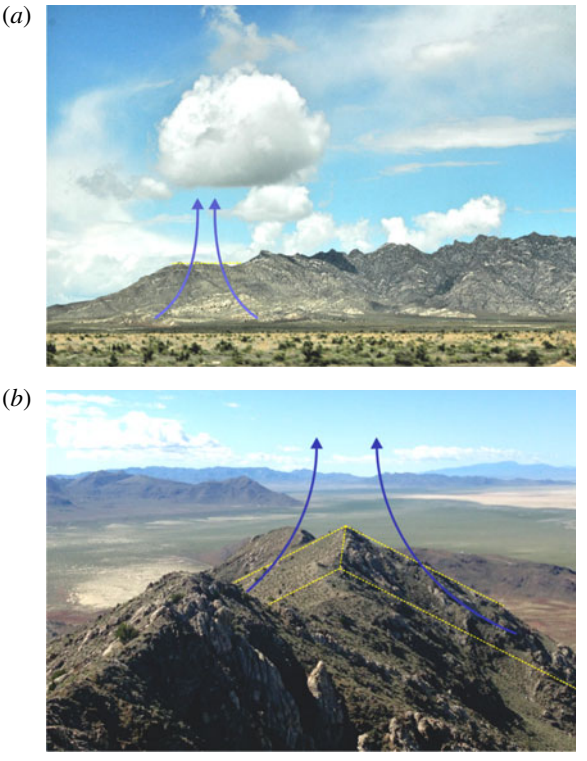


FIGURE 9. (Colour online) Granite Mountain, Utah with (*a*) frequently occurring solitary cumulus cloud formation directly over the peak (Courtesy: L. S. Leo) and (*b*) the LiDAR scan location revealing the quasi-symmetry.

mountain, which is on average 11.8 km long, 6.1 km wide and 0.6 km high. The area surrounding the mountain was densely instrumented with a suite of point and remote sensors (Fernando *et al.* 2015). Observations were made during two major field experiments conducted during October 2012 and May 2013. Climatologically, the autumn experiment was intended to study quiescent days characterized by high pressure (low synoptic) conditions and the spring campaign was focused on synoptic days characterized by significant background winds.

During quiescent days with moderate to high sunshine and sufficient moisture, a solitary cumulus cloud was almost always observed directly above a peak of the Granite Mountain (figure 9*a*), indicating the possibility of a separated flow from below. Upon further investigation it was found that the peak is quasi-symmetric (figure 9*b*), the slope was nominally 2D over horizontal distances of $\sim$1.5 km, and the north to south peak orientation provided equivalent early afternoon eastern and western slope sun exposure, thus satisfying the model assumptions of § 5 to a reasonable degree. Although the site was not in the experimental plan for siting instrumentation, special arrangements were made during the spring campaign to relocate a Doppler LiDAR (laser-Radar) to this site for a limited time for observations outside (synoptic-wind focused) the intense observational periods. The number of low-synoptic days with useful data, however, was limited during the spring experiments. Anticipating stronger winds, the tethered balloon flights were not included as part of the spring instrumentation. As such, the background stratification could not be measured directly,

https://doi.org/10.1017/jfm.2015.298 Published online by Cambridge University Press

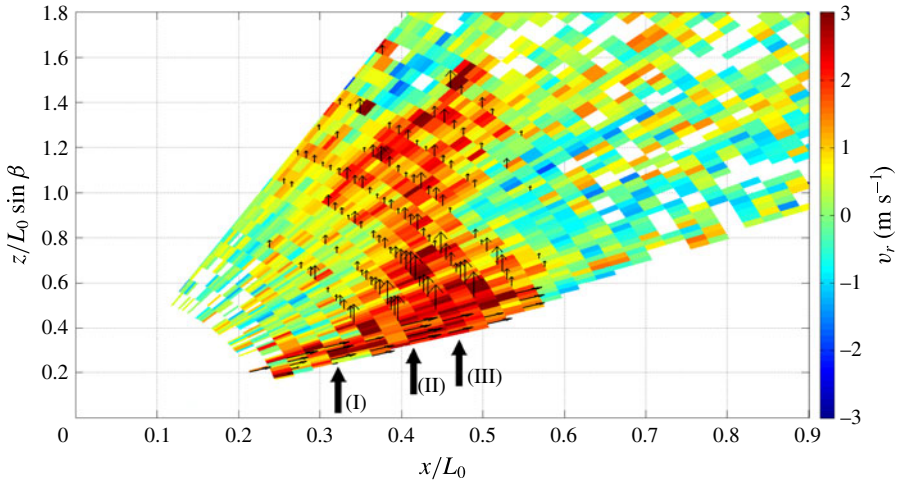


FIGURE 10. Doppler wind LiDAR scan of separating upslope flow, where the radial velocity is coloured with vectors overlaid. No vectors are presented where neither u nor w can be neglected. The flow can be decomposed into three zones, (I) the upslope flow, (II) approximate separation point and (III) plume region. The data were taken on 30 May 2013.

but a microwave radiometer located 15 km away in the valley indicated that the boundary layer was well mixed up to about 2 km on the days of measurements. Data on a suite of meteorological towers and remote sensors are available from all of the MATERHORN experiments, and are presented elsewhere (Fernando *et al.* 2015).

The LiDAR was positioned at the base of the slope, and was aligned to continuously scan parallel to the mean upslope flow direction, sweeping from the base of the incline towards the peak and beyond, with each scan taking 17 s to complete. There were only three days of low-synoptic conditions during the deployment period. Since the LiDAR beam scan is parallel to the mean flow direction, the (x, z) flow components (u, w) can be projected onto the measured radial Doppler velocity, $u_r = u\cos\theta + w\sin\theta$, where θ is the scanner elevation angle from the horizontal. Within the upslope flow boundary layer, w can be assumed small such that the upslope velocity $U \sim u_r/\cos(\theta - \beta)$, while outside the upslope flow boundary layer, the upslope velocity goes to zero and $w \sim u_r/\sin\theta$. A LiDAR scan of the separating upslope flow is shown in figure 10, in which the radial velocity is coloured while the vectors are overlaid to show the approximate direction of the flow. The determination of the separation point is somewhat subjective as evident from figure 10, due to the limitations of measurement resolution near the surface; we therefore opted to estimate the separation point as the location where the maximum vertical velocity is first found.

The estimated dimensionless separation distance is $L_s/L_0 = 0.45 \pm 0.025$ (± 1 LiDAR range gate), where the slope length is $L_0 = 712$ m. Observations over three days of cumulus formation confirmed the separation distance result within 10 %. Comparison with the model, however, is somewhat problematic, given the change of slope angle in the field from $\beta = 16.5^\circ$ at the base to $\beta = 23^\circ$ at the peak, a complication that is absent in the model. A possibility is to use a mean slope, $\beta = 19.8^\circ$, and evaluate the separation distance using (5.8) as $L_s/L_0 = 0.52$ with an uncertainty of ± 0.02. Nonetheless, as kindly pointed out by a referee, the model is invalid for

https://doi.org/10.1017/jfm.2015.298 Published online by Cambridge University Press

$\beta \leqslant 20°$, and hence it more appropriate to use the empirically determined separation distance for $\beta \approx 20°$ based on figure 6, which is $L_s/L_0 \approx 0.47 \pm 0.02$. Although the agreement is excellent, it should be viewed with circumspection because of the complicating factors present, such as variable slope, possible influence of atmospheric stability particularly at greater elevations and the slope roughness in nature that might increase the boundary-layer thickness (Britter *et al.* 1981). The stable stratification reduces the likelihood of separation while a higher surface roughness may decrease the shear-induced vorticity U_s/δ that keeps the flow attached. Future laboratory experimental and numerical work should consider such effects in detail.

7. Conclusions

Laboratory experiments were performed to investigate the separation of thermally driven upslope flow on isolated 2D mountains under neutrally stratified, quiescent background conditions. The experiments were performed in a water tank, with the slope spanning the entire width of the tank and heated by special heating elements. Particle tracking velocimetry (PTV) augmented by feature tracking visualization (FTV) was used for flow diagnostics. A full range of slope angles and heat fluxes were utilized. The interest was on flow structures, the upslope flow separation distance, and the velocity field at different locations of interest. Upon initiation of heating, the flow underwent a transition period characterized by convective instabilities at the heating surface and unsteady upslope flow development. This was followed by a quasi-steady flow regime devoid of endwall influence, during which a warmer fluid intrusion at the top of the tank propagated away from the slope region while the upslope flow and separated plume was approximately steady. Upon the intrusion reaching the endwall, the flow in the tank was found to be dominated by wall effects. The emphasis of our work was on the quasi-steady regime.

Three different flow regimes were identified. When the slope angle $\beta > \beta_c$ ($\approx 20°$), the flow in the vicinity of the separation point appeared to be fed entirely by the anterior upslope flow. When $\beta \leqslant \beta_c$, the plume emanating at the separation point could not be fully supplied by the upslope flow, and hence additional entrainment of ambient fluid was evident in the separation area (plume source). The separation distance was appreciably reduced under these conditions. When $\beta \leqslant 10°$, the rising plume engulfed most of the slope, similar to a plume rising from a horizontal area source of finite extent. For that case, the entrainment flow penetrated over the source (slope) for about $L_s \approx 0.2L_0$, before being overpowered by and melded into rising plumes.

Assuming that the separation point is determined by the opposing vorticity contributions of baroclinic torque (characterizing the separation tendency) and boundary-layer shear (attachment), a model was developed to predict the normalized separation length L_s/L_0 from the base of the mountain for $\beta > \beta_c$, which predicted that L_s/L_0 is a function of only β under conditions of Reynolds number similarity. The velocity and length scales at the separation as well as the scaling for the separated plume were derived. The theoretical predictions compared favourably with the laboratory data for $\beta > \beta_c$, and the Reynolds number similarity was confirmed.

Comparisons were made between the model predictions and Doppler wind LiDAR field measurements taken during the days of near-neutral stratification of the MATERHORN field program. However, the averaged slope of the field site was smaller than β_c, restricting the use of the model prediction (5.8). Since dimensional analysis indicates that in general $L_s/L_0 = f_2(\beta)$, the laboratory measurements for $\beta \leqslant \beta_c$ could be used for comparisons. The agreement between laboratory-based

https://doi.org/10.1017/jfm.2015.298 Published online by Cambridge University Press

predictions and MATERHORN observations was excellent, notwithstanding the field site having gradually varying topography, surface heterogeneities and possible residual stratification. The applicability of laboratory water tank results to the atmospheric cases has been demonstrated by Chen *et al.* (1999) via a detailed analysis of the governing equations of motion.

The present work did not consider background stratification, and therefore mimicked atmospheric conditions only after the breakup of inversion during morning transition. Therefore, our results are inapplicable to upslope flows occurring in the early morning, for example, for the case considered by Princevac & Fernando (2008) or when a residual stable stratification is present throughout the day. In such cases, the flow separation is either suppressed or a new separation mechanism arises in the form of intrusions separating out of the upslope flow (Lu & Turco 1994; Princevac & Fernando 2008). The suppression of separation by stratification is also indicated in the numerical simulations of Serafin & Zardi (2010*a*), which considered heating of a symmetric 2D mountain ridge with $\beta = 30^\circ$ immersed in linearly stratified air. Flow separation was evident (their figure 8) without intrusion formation, with L_s/L_0 values larger than that predicted by our model ($\approx$0.6).

Mountain terrain weather is among the most difficult to predict, and flow separation that leads to strong updrafts and deep convection was a topic of considerable interest studied in the MATERHORN (2011–2016) program. It is hoped that the present work will contribute towards interpreting field and modelling studies that have been conducted under a large number of research programs dealing with complex terrain weather, conducted by a large number of research groups (Fernando *et al.* 2015).

Acknowledgements

This research was funded by the Office of Naval Research Award no. N00014-11-1-0709, mountain terrain atmospheric modelling and observations (MATERHORN) Program. We sincerely thank three anonymous referees for providing careful and useful insights that led to substantial improvement of this paper.

REFERENCES

ALLEN, T. & BROWN, A. R. 2006 Modeling of turbulent form drag in convective conditions. *Boundary-Layer Meteorol.* **118**, 421–429.

APSLEY, D. D. & CASTRO, I. P. 1997 A limited-length-scale k–ε model for the neutral and stably-stratified atmospheric boundary layer. *Boundary-Layer Meteorol.* **83**, 75–98.

BAINES, P. G. 1995 *Topographic Effects in Stratified Flows*. Cambridge University Press.

BAINES, P. G. & MANINS, P. C. 1989 The principles of laboratory modeling of stratified atmospheric flows over complex terrain. *J. Appl. Meteorol.* **28**, 1213–1225.

BANTA, R. M. 1984 Daytime boundary-layer evolution over mountainous terrain. Part I: observations of the dry circulations. *Mon. Weath. Rev.* **112**, 340–356.

BARRY, R. G. 1992 *Mountain Weather & Climate*. Routledge.

BELCHER, S. E. & HUNT, J. C. R. 1998 Turbulent flow over hills and waves. *Annu. Rev. Fluid Mech.* **30**, 507–538.

BERMAN, N. S., BOYER, D. L., BRAZEL, A. J., BRAZEL, S. W., CHEN, R. R., FERNANDO, H. J. S. & FITCH, M. J. 1995 Synoptic classification and physical model experiments to guide field studies in complex terrain. *J. Appl. Meteorol.* **34**, 719–730.

BLUMEN, W. 1990 *Atmospheric Processes over Complex Terrain*, Meteorological Monographs, vol. 23. American Meteorological Society

BOYER, D. L. & DAVIES, P. A. 2000 Laboratory studies of orographic effects in rotating and stratified flows. *Annu. Rev. Fluid Mech.* **32**, 165–202.

https://doi.org/10.1017/jfm.2015.298 Published online by Cambridge University Press

BRITTER, R. E., HUNT, J. C. R. & RICHARDS, K. J. 1981 Air flow over a two-dimensional hill: studies of velocity speed-up, roughness effects and turbulence. *Q. J. R. Meteorol. Soc.* **107**, 91–110.

CARRUTHERS, D. J., ELLIS, A., HUNT, J. C. R. & CHAN, P. W. 2014 Modeling of wind shear downwind of mountain ridges at Hong Kong International Airport. *Meteorol. Appl.* **21** (1), 94–101; (special issue).

CHAO, W. C. 2012 Correction of excessive precipitation over steep and high mountains in a GCM. *J. Atmos. Sci.* **69**, 1547–1561.

CHEN, C. C., LABHABI, A., CHANG, H. C. & KELLY, R. E. 1991 Spanwise pairing of finite-amplitude longitudinal vortex rolls in inclined free-convection boundary layers. *J. Fluid Mech.* **231**, 73–111.

CHEN, R. R., BERMAN, N. S., BOYER, D. L. & FERNANDO, H. J. S. 1996 Physical model of diurnal heating in the vicinity of a long mountain. *J. Atmos. Sci.* **53**, 62–85.

CHEN, R. R., BERMAN, N. S., BOYER, D. L. & FERNANDO, H. J. S. 1999 Physical model of nocturnal drainage flow in complex terrain. *Contrib. Atmos. Phys.* **72**, 219–242.

COLOMER, J., BOUBNOV, B. M. & FERNANDO, H. J. S. 1999 Turbulent convection from isolated sources. *Dyn. Atmos. Oceans* **30**, 125–148.

CROOK, N. A. & TUCKER, D. F. 2005 Flow over heated terrain. Part I: Linear theory and idealized numerical simulations. *Mon. Weath. Rev.* **133**, 2552–2564.

DE WEKKER, S. F. 2008 Observational and numerical evidence of depressed convective boundary layer height near a mountain base. *J. Appl. Meteorol. Climatol.* **47**, 1017–1026.

DÖRNBRACK, A. & SCHUMANN, U. 1993 Numerical simulation of turbulent convective flow over wavy terrain. *Boundary-Layer Meteorol.* **65**, 323–355.

DOYLE, J. D. & DURRAN, D. R. 2007 Rotor and subrotor dynamics in the lee of three-dimensional terrain. *J. Atmos. Sci.* **64**, 4202–4221.

ELLIS, A. W., HILDEBRANDT, M. L., THOMAS, W. M. & FERNANDO, H. J. S. 2000 Analysis of the climatic mechanisms contributing to the summertime transport of lower atmospheric ozone across metropolitan Phoenix, Arizona, USA. *Clim. Res.* **15**, 13–31.

FERNANDO, H. J. S. 2010 Fluid dynamics of urban atmospheres in complex terrain. *Annu. Rev. Fluid Mech.* **42**, 365–389.

FERNANDO, H. J. S., LEE, S. M., ANDERSON, J., PRINCEVAC, M., PARDYJAK, E. & GROSSMAN-CLARKE, S. 2001 Urban fluid mechanics: air circulation and contaminant dispersion in cities. *Environ. Fluid Mech.* **1**, 107–164.

FERNANDO, H. J. S. & PARDYJAK, E. R. 2013 Field studies delve into the intricacies of mountain weather. *Eos* **94** (36), 313–315.

FERNANDO, H. J. S., PARDYJAK, E., DI SABATINO, S., CHOW, F. K., FERNANDO, H. J. S., PARDYJAK, E. R., DI SABATINO, S., CHOW, F. K., DE WEKKER, S. F. J., HOCH, S. W., HACKER, J., PACE, J. C., PRATT, T., PU, Z., STEENBURGH, J. W., WHITEMAN, C. D., WANG, Y., ZAJIC, D., BALSLEY, B., DIMITROVA, R., EMMITT, G. D., HIGGINS, C. W., HUNT, J. C. R., KNIEVEL, J. C., LAWRENCE, D., LIU, Y., NADEAU, D. F., KIT, E., BLOMQUIST, B. W., CONRY, P., COPPERSMITH, R. S., CREEGAN, E., FELTON, M., GRACHEV, A., GUNAWARDENA, N., HANG, C., HOCUT, C. M., HUYNH, G., JEGLUM, M. E., JENSEN, D., KULANDAIVELU, V., LEHNER, M., LEO, L. S., LIBERZON, D., MASSEY, J. D., MCENERNEY, K., PAL, S., PRICE, T., SGHIATTI, M., SILVER, Z., THOMPSON, M., ZHANG, H. & ZSEDROVITS, T. 2015 The MATERHORN – unraveling the intricacies of mountain weather. *Bull. Am. Meteorol. Soc.* (in press); doi:10.1175/BAMS-D-13-00131.1.

FERNANDO, H. J., ZAJIC, D., DI SABATINO, S., DIMITROVA, R., HEDQUIST, B. & DALLMAN, A. 2010 Flow, turbulence, and pollutant dispersion in urban atmospheres. *Phys. Fluids* **22** (5), 051301.

GEERTS, B., MIAO, Q. & DEMKO, J. C. 2008 Pressure perturbations and upslope flow over a heated, isolated mountain. *Mon. Weath. Rev.* **136**, 4272–4288.

GONG, W. & IBBETSON, A. 1989 A wind tunnel study of turbulent flow over model hills. *Boundary-Layer Meteorol.* **49**, 113–148.

https://doi.org/10.1017/jfm.2015.298 Published online by Cambridge University Press

HANLEY, K. E., KIRSHBAUM, D. J., BELCHER, S. E., ROBERTS, N. M. & LEONCINI, G. 2011 Ensemble predictability of an isolated mountain thunderstorm in a high resolution model. *Q. J. R. Meteorol. Soc.* **137**, 2124–2137.

HEWER, F. E. 1998 Non-linear numerical model predictions of flow over an isolated hill of moderate slope. *Boundary-Layer Meteorol.* **87**, 381–408.

HUNT, J. C. R. 1991 Industrial and environmental fluid mechanics. *Annu. Rev. Fluid Mech.* **23**, 1–42.

HUNT, J. C. R., FERNANDO, H. J. S. & PRINCEVAC, M. 2003 Unsteady thermally driven flows on gentle slopes. *J. Atmos. Sci.* **60**, 2169–2182.

HUNT, J. C. R., LEIBOVICH, S. & RICHARDS, K. J. 1988 Turbulent shear flows over low hills. *Q. J. R. Meteorol. Soc.* **114**, 1435–1470.

JACKSON, P. S. & HUNT, J. C. R. 1975 Turbulent wind flow over low hills. *Q. J. R. Meteorol. Soc.* **101**, 929–955.

KLINE, S. J. & MCCLINTOCK, F. A. 1953 Describing uncertainties in single-sample experiments. *Mech. Engng* **75**, 3–8.

KRETTENAUER, K. & SCHUMANN, U. 1989 Direct numerical simulation of thermal convection over a wavy surface. *Meteorol. Atmos. Phys.* **41**, 165–179.

LEHNER, M. & WHITEMAN, C. D. 2012 The thermally driven cross-basin circulation in idealized basins under varying wind conditions. *J. Appl. Meteorol.* **51**, 1026–1045.

LEWIS, H. W., MOBBS, S. D., VOSPER, S. B. & BROWN, A. R. 2008 The effect of surface heating on hill-induced flow separation. *Boundary-Layer Meteorol.* **129**, 269–287.

LIGHTHILL, M. J. 1963 Introduction: boundary layer theory. In *Laminar Boundary Theory* (ed. L. Rosenhead), pp. 46–113. Oxford University Press.

LIST, E. J. 1982 Turbulent jets and plumes. *Annu. Rev. Fluid Mech.* **14**, 189–212.

LU, R. & TURCO, R. P. 1994 Air pollutant transport in a coastal environment. Part 1: 2-D simulations of sea breeze and mountain effects. *J. Atmos. Sci.* **51**, 2285–2308.

MASON, P. J. 1987 Diurnal variations in flow over a succession of ridges and valleys. *Q. J. R. Meteorol. Soc.* **113**, 1117–1140.

MASON, P. J. & KING, J. C. 1985 Measurements and predictions of flow and turbulence over an isolated hill of moderate slope. *Q. J. R. Meteorol. Soc.* **111**, 617–640.

MOREIRA, G. A. A., DOS SANTOS, A. A. C., DO NASCIMENTO, C. A. M. & VALLE, R. M. 2012 Numerical study of the neutral atmospheric boundary layer over complex terrain. *Boundary-Layer Meteorol.* **143**, 393–407.

PAPANICOLAOU, P. N. & LIST, E. J. 1988 Investigations of round vertical turbulent buoyant jets. *J. Fluid Mech.* **195**, 341–391.

PARDYJAK, E. R., FERNANDO, H. J. S., HUNT, J. C. R., GRACHEV, A. A. & ANDERSON, J. 2009 A case study of the development of nocturnal slope flows in a wide open valley and associated air quality implications. *Meteorol. Z.* **18** (1), 85–100.

POLITOVICH, M. K., GOODRICH, R. K., MORSE, C. S., YATES, A., BARRON, R. & COHN, S. A. 2011 The Juneau terrain-induced turbulence alert system. *Bull. Am. Meteorol. Soc.* **92** (March), 299–313.

PRINCEVAC, M. & FERNANDO, H. J. S. 2007 A criterion for the generation of turbulent anabatic flows. *Phys. Fluids* **19**, 105102.

PRINCEVAC, M. & FERNANDO, H. J. S. 2008 Morning break-up of cold pools in complex terrain. *J. Fluid Mech.* **616**, 99–109.

QUENEY, P. 1948 The problem of air flow over mountains: a summary of theoretical studies. *Bull. Am. Meteorol. Soc.* **29**, 16–26.

RAUPACH, M. R. & FINNIGAN, J. J. 1997 The influence of topography on meteorological variables and surface-atmosphere interactions. *J. Hydrol.* **190**, 182–213.

RAYMOND, D. J. 1972 Calculation of airflow over an arbitrary ridge including diabatic heating and cooling. *J. Atmos. Sci.* **29**, 837–843.

REISNER, J. M. & SMOLARKIEWICZ, P. K. 1994 Thermally forced low Froude number flow past three-dimensional obstacles. *J. Atmos. Sci.* **51**, 117–133.

https://doi.org/10.1017/jfm.2015.298 Published online by Cambridge University Press

REUTEN, C., STEYN, D. G. & ALLEN, S. E. 2007 Water tank studies of atmospheric boundary layer structure and air pollution transport in upslope flow systems. *J. Geophys. Res.* **112**, D11114.

REUTEN, C., STEYN, D. G., STRAWBRIDGE, K. B. & BOVIS, P. 2005 Observations of the relation between upslope flows and the convective boundary layer in steep terrain. *Boundary-Layer Meteorol.* **116**, 37–61.

ROUSE, H., YIH, C. S. & HUMPHREYS, H. W. 1952 Gravitational convection from a boundary source. *Tellus* **4**, 201–210.

SCHUMANN, U. 1989 Large-eddy simulation of the up-slope boundary layer. *Q. J. R. Meteorol. Soc.* **116**, 637–670.

SCORER, R. S. 1997 *Dynamics of Meteorology and Climate*. Wiley.

SERAFIN, S. & ZARDI, D. 2010*a* Structure of the atmospheric boundary layer in the vicinity of a developing upslope flow system: a numerical model study. *J. Atmos. Sci.* **67**, 1171–1185.

SERAFIN, S. & ZARDI, D. 2010*b* Daytime heat transfer processes related to slope flows and turbulent convection in an idealized mountain valley. *J. Atmos. Sci.* **67**, 3739–3756.

SMITH, R. B. & LIN, Y. L. 1982 The addition of heat to a stratified airstream with application to the dynamics of orographic rain. *Q. J. R. Meteorol. Soc.* **108**, 353–378.

TAYLOR, P. A. & TEUNISSEN, H. W. 1987 The Askervein Hill project: overview and background data. *Boundary-Layer Meteorol.* **39**, 15–39.

TIAN, W. & PARKER, D. J. 2003 A modeling study and scaling analysis of orographic effects on boundary layer shallow convection. *J. Atmos. Sci.* **60**, 1981–1991.

WHITEMAN, C. D. 2000 *Mountain Meteorology: Fundamentals and Applications*. Oxford University Press.

WOOD, N. 1995 The onset of separation in neutral, turbulent flow over hills. *Boundary-Layer Meteorol.* **76**, 137–164.

XU, D., AYOTTE, K. W. & TAYLOR, P. A. 1994 Development of a non-linear mixed spectral finite difference model for turbulent boundary-layer flow over topography. *Boundary-Layer Meteorol.* **70**, 341–367.

https://doi.org/10.1017/jfm.2015.298 Published online by Cambridge University Press